Contribution of static light scattering to the textural characterisation of large aggregates

Mohamed Bizi, Gérard Baudet

HAL Id: hal-00715339

https://brgm.hal.science/hal-00715339

Submitted on 6 Jul 2012

Contribution of static light scattering to the textural characterization of large aggregates

M. Bizi[*], G. Baudet

BRGM Environment & Processes Division, 3, Avenue C. Guillemin, 45060 ORLEANS Cedex 2, France

* Corresponding author.
E-mail address: m.bizi@brgm.fr
Phone +33(0)2 38 64 36 62

Abstract

The industrial processes of water clarification often imply flocs of millimetre length. The principal motivation of this work relates to the characterization of these large flocs with laser diffractometry, for which the authors propose particular experimental approaches. In addition, a reformulation of the various properties of the flocs accessible by laser diffractometry is presented, in particular for the determination of the size, density, porosity, volume fraction and fractal dimension. By way of illustration, these experimental and theoretical developments are applied to the characterization of flocs obtained by flocculation of a commercial kaolin. The size, fractal dimension and density of kaolin floc were examined under various flocculant concentrations. Measurements reveal important variations of the granulometric and textural properties of large size flocs in response to flocculation, opening ways of optimization for the associated industrial processes.

KeyWords: Density; Floc size distribution; Fractal dimension; Kaolin; Light scattering; Obscuration; Porosity.

---

1. Introduction

Flocculation is the process by which disperse solid or microbial elementary units aggregate as flocs under the effects of a chemical reagent. The efficiency of the flocculation is assessed in terms of i) water quality, ii) post-processing state of the sediment obtained and iii) the swiftness of the physical and chemical process selected. For a given material and water, these three assessment criteria depend on the nature of the reagent and on the hydrodynamic conditions used – and accordingly on the texture of the floc produced.

Thus, water purification depends on the possibility of aggregating all the particles into flocs and on the sedimentation rate of the flocs that have been formed; the latter is a function of both their size and their density. The settling of the sediment is linked with the mechanical properties of the flocs and with their porosity. Furthermore, many investigations have made it possible to associate the fractal structure of the flocs with various physical and chemical properties such as decantation [1-3], growth [4] and diffusion [5]. Size, density, porosity and fractal dimension can thus be considered as representative of the overall flocculation efficiency.

Taking into account the fact that flocs are extremely fragile structures, they accordingly need to be characterised in terms of size, density, porosity and fractal dimension by means of methods that are direct and non-destructive. For practical reasons we propose to use laser scattering to cover, in terms of textural characterization, a range of aggregates linked with several types of industry. The sizes targeted are those of flocs produced industrially, ranging between 0.01 and 5 mm. In conformity with this objective, the study was subdivided into three parts. The first part develops the parameters of theoretical bases necessary to describe the texture of the flocs. The second part relates to the development of a system for the analysis of large size flocs using laser diffractometry. The third part, essentially experimental, proposes an application of the developments of the two preceding parts to the characterization of large flocs obtained by flocculation of a commercial kaolin.

2. Static light scattering characterization

Over the past 30 years, laser diffractometry has become the reference technique for determining size in fine-grained materials. The fundamental principles of this technique have been dealt with in detail in a number of reports or publications [7, 8]. It presents a number of advantages over classical methods such as electron microscopy or X-ray absorption (Sedigraph). It is fast, reproducible, easy to use, and inexpensive and yields several types of textural information: size, shape coefficient of lamellar particles, external surface geometry [9], and the porosity, density, fractal dimension of the flocs [10-12]. Its main drawback is linked to the limitations, inherent to the Fraunhofer and Lorentz-Mie theories used to interpret the diffraction and diffusion patterns. As explained below, both these theories were designed for spherical particles. In addition, for the principles of Fraunhofer to be applied, the particles must be opaque and larger than $5\lambda_0$, or otherwise, for the Lorentz-Mie theory to be used, they must have well-known optical properties. As in all the other techniques, the size distributions are established accordingly to the model of the equivalent sphere. In the light of its specificities, laser diffractometry is complementary to the other techniques.

2.1 Size, porosity and density of the flocs obtained by laser diffractometry

The underlying principle behind laser diffractometry is the exploitation of the information contained in the light scattered by the particles that examined subsequent to their interaction with a TEM_{00}-type electromagnetic plane wave. The amount of light scattered and the size of the angle of diffusion allow us to determine the size of the particles and their relative quantity. This data can be extracted by applying the Lorentz-Mie theory on the condition of respecting that certain hypotheses are satisfied and that the optical properties of the material being analysed are known. Thus the particles are supposed to be spherical, isotropic, homogenous and non-magnetic. In practice, the investigated materials are actually not suitable with this definition: they are neither spherical nor isotropic, and rarely their optical properties are known. In the field of flocculation/coagulation, the situation is even more complicated. As compared with a raw product, the flocs display an optical contrast with respect to the transport fluid that varies widely according to the amount of flocculant and the structure of the flocs. In this context, the Fraunhofer model, a special case of the Lorentz-Mie theory, must be called on to interpret the signals. It makes it possible to determine the size distribution of the particles, taken to be spherical and opaque, from photometric measurements. This model represents a good approximation for particles whose diameters are five times greater than the wavelength λ_0 of the incident beam. If the ratio diameter/wavelength is smaller than 5, the errors are liable to be large, and the distributions should be considered as relative value rather than absolute. However, when the flocculation of fine particles ($<5\lambda_0$) is concerned, the level of error decreases with increasing size and compactness (fractal dimension) of the flocs, which is true for the flocculation in the present study.

The Fraunhofer model, present on all laser particle size analysers (PSA's), is based on the principle of light scattering [13,14]. In the case of the Mastersizer-S PSA used here, the helium-neon laser, with a wavelength of 0.632 µm, emits a beam that is broadened by means of an afocal optic system equipped with a spatial filter. This beam, 18 mm in diameter, passes through a liquid film of width ℓ crossing an analysis cell where the particles to be measured are dispersed. The particles, assumed to be opaque, diffract the light according to an angle inversely proportional to their diameter, and the diffraction pattern centred on the image of the source depends neither on position nor on particle motion. Each granulometric class centred on a diameter d_i has its own diffraction pattern. If all the particles are of the same size, the resultant pattern is that of Airy, which appears as a succession of concentric rings. The size of these identical particles is deduced from that of these rings. However, when the material is polydisperse, the elementary diffraction patterns superimpose on each other in the focal plane, and the rings disappear. The size distribution is determined from the irradiance (diffracted energy) received by the detector head. For the PSA used here, the detector is composed of 42 silicon photodiodes arranged along concentric arcs. In the standard range that is usable in wet treatment (from 0.05 to 880 µm), all the photodiodes are called on for size measurement. On the other hand, for the 4.2 to 3480 µm, only the first 32 diodes are used. In both cases, each photodiode is allotted to a particle-size range. The mode of calculation of the size distribution is largely treated in the literature. It will not be included in this work. The result of the measurement analysis is a volume distribution characterised over the size limits of the optical configuration used. The distribution may be listed as a table of results, giving frequency and cumulative forms of distribution.

Moreover, the particle-measurement instrument is equipped with a central detector (0°) devoted to the measurement of obscuration i.e., attenuation of laser beam by the sample. This obscuration is deduced from measurement from intensity of the central beam I_C by neglecting the diffusion in front of absorption.

$$Ob = 1 - \frac{I_c}{I_0} \qquad (1)$$

$$I_c = I_0 \exp\left(-\tau.\ell\right) \qquad \text{Beer-Lambert law} \qquad (2)$$

$$\tau = \sum N_i \cdot A_i.Q_{ext.i} \qquad (3)$$

where

Ai	projected area of the size band i;
I_c	intensity received on central detecror;
I_0	intensity emitted by the laser (received in absence of particles);
ℓ	optical path length;
N_i	number of particles of size band i per unit volume;
Ob	obscuration of the light;
$Q_{ext,i}$	extinction efficiency (for Fraunhofer diffraction, it is equal to 2);
τ	particle field turbidity.

As indicated above, obscuration is a function of the optical trajectory ℓ and of the turbidity of the medium τ, which itself is a function of the concentration (or number of particles) and of the efficient extinction factor Q_{ext} (the ratio between the energy flux drawn from the incident wave and the energy flux received by the geometric section of the particle). Through this factor, obscuration also depends on the size parameter α and on the complex refractive index of the medium n_m in which the wave is propagating. The connection between Q_{ext} and these parameters lies beyond the scope of this work. The relations and approximations assigned to this factor are widely dealt with in the literature [15,16]. However, its limit tends towards 2 for large values of α (the field of application of Fraunhofer).

$$\alpha = \frac{2.\pi}{\lambda_0}.r_0 \qquad (4)$$

For a cloud of spherical, isotropic, homogenous, nonmagnetic and monodisperse particles, turbidity can be defined by [16]

$$\tau = \frac{3}{2} \cdot \frac{C}{\rho_S.d_{3.2}}.\overline{Q_{ext}} \qquad (5)$$

which shows fairly clearly that, for a given optical trajectory, obscuration increases to a certain extent as the concentration increases. On the other hand, for a given concentration and optical trajectory, obscuration decreases when particle size increases.

In the case of the polydisperse spherical particles, the turbidity is computed from the relative volumes of the different size classes, V_{ri}, and the volume concentration C/ρ, noted C_v. The projected surface area of a size class with volume V_i and diameter d_i is given in the present case by the following relation:

$$N_i.A_i = \frac{3}{2}.\frac{V_i}{d_i} \qquad (6)$$

The volume corresponding to a class i is written:

$$V_{ri} = \frac{V_i}{V_{SB}}.V_B \qquad (7)$$

so,

$$V_i = \frac{V_{SB}}{V_B}.V_{ri} \quad \text{and} \quad N_i.A_i = \frac{3}{2}.\frac{V_{ri}}{d_i}.\frac{V_{SB}}{V_B} \qquad (8)$$

where

A_i	projected area of the size band i;
C	concentration expressed as grams per millilitre;
C_V	particle volume concentration measured by the granulometer (volume of all particles per volume of suspension containing these particles);
$d_{3.2}$	Sauter mean diameter;
N_i	number of particles of size band i per unit volume;
$\overline{Q_{ext}}$	average extinction efficiency;
r_0	radius of the primary particle (monodisperse);
V_B	beam volume, which is the cross-sectional area times the path length;
V_{ri}	relative volume of particles in size band i per unit volume;
V_{SB}	total volume of all solid scattering particles in the beam;
ρ_S	density of particulate matter expressed as grams per cm^3.

Substituting for $N_i.A_i$ its last expression in Eq. (3), the turbidity becomes

$$\tau = \frac{3}{2} \cdot \frac{V_{SB}}{V_B} \cdot \sum \frac{V_{ri}}{d_i} \cdot Q_{ext.i} \qquad (9)$$

The ratio $\dfrac{V_{SB}}{V_B}$ represents the volume concentration, C_V.

Combining Eqs. (2) and (9) allows the final expression of the volume concentration measured by laser light scattering to be established:

$$C_V = \frac{V_{SB}}{V_B} = \frac{\ln\left(\dfrac{I_c}{I_0}\right)}{\dfrac{-3}{2} \cdot \ell \cdot \sum \dfrac{V_{ri} Q_{ext.i}}{d_i}} \qquad (10)$$

This relation can be used to determine the volume concentration from a measurement of the transmittance I_c/I_0 and the computed turbidity. However, it may prove not to be applicable for a number of reasons. Thus, the proportionality between obscuration and concentration is correctly verified only over a particular range of concentrations which ensures multiple scattering and practically non-existent mask effects. The rules for using this relationship will be detailed in Section 4.1.

However, textural characterization by the laser diffractometry of porous materials (aggregates or flocs) measuring C_V makes it possible to determine the mean porosity and the effective volume-specific mass of these materials. The technique is fast, reproducible, statistically representative and relatively reliable in comparison with the classical indirect methods derived from the Stokes law. These classical methods consist in linking the fall rate of the flocculated particles and their diameter to the Stokes equation, corrected in terms of the Reynolds number and the shape factor of the particles. The diameters are often determined by image analysis. This correction must take into account the permeability and the shape of the flocs, which evolve with the physical and chemical and hydrodynamic conditions. Another worthy technique is the assessment of effective volume-specific mass from the measurement of the volume and the mass of the flocs using micro scales. Typically, these methods are time-consuming and costly.

In textural characterization, porosity is defined by

$$\varepsilon_F = \frac{V_{SB} - V_{SR}}{V_{SB}} \qquad (11)$$

where V_{SB} is the volume of porous entities intercepted by the laser beam, corresponding to the sum of the real volume of the solid V_{SR} and of the flocs porosity.

$$V_{SB} = V_B.C_V \quad \text{and} \quad V_{SR} = V_B.\frac{C}{\rho_S} \tag{12}$$

Therefore, the average porosity is defined according to the value C_V measured by PSA.

$$\varepsilon_F = 1 - \frac{C}{(C_V \cdot \rho_S)} \tag{13}$$

The result is the following expression of the average density of porous materials such as flocs:

$$\rho_F = \rho_S \cdot (1 - \varepsilon_F) + \rho_L \cdot \varepsilon_F \tag{14}$$

The porosity and the density obviously depend on the number of particles an aggregate contains. This number varies, increasing with increasing size of the aggregate R. It depends on the aggregate's structure, and accordingly on its fractal dimension. These relationships are incorporated into the following equation

$$n(r) = k_0 \left(\frac{R}{r_0} \right)^{D_F} \tag{15}$$

where

D_F average fractal dimension;
n number of primary particles in an aggregate;
k_0 fractal prefactor, which is a function of the average size of primary particle;
r_0 radius of the primary particle (monodisperse);
R radius of the aggregate.

This equation is defined over a size range varying between that of the elementary particle and that of the aggregate. From this relation derives any number of useful expressions linking to various properties of the aggregate with its fractal dimension. The porosity of the fractal aggregate, for instance, is a function of its size:

$$\varepsilon_F(r) = 1 - \frac{V_{SR}}{V_{SB}} = 1 - n(r) \cdot \frac{V_0}{V_{SB}} \tag{16}$$

For spheres, $\qquad V_{SB} = \frac{4}{3}\pi R^3 \tag{17}$

$$V_0 = \frac{4}{3}\pi r_0^3 \tag{18}$$

$$\frac{V_0}{V_{SB}} = \left(\frac{r_0}{R} \right)^3 \tag{19}$$

so : $\qquad \varepsilon(r) = 1 - k_0 \left(\frac{R}{r_0} \right)^{D_F - 3} \tag{20}$

The complement to the porosity is the solid volume fraction, that is,

$$\Phi_F = 1 - \varepsilon_F = k_0 \cdot \left(\frac{R}{r_0} \right)^{D_F - 3} \tag{21}$$

$$\rho_F = \rho_L + (\rho_S - \rho_L) \cdot k_0 \cdot \left(\frac{R}{r_0} \right)^{D_F - 3} \tag{22}$$

This equation shows that floc density decreases with increasing floc size, roughly in accordance with a power-law relationship between density and size. It will be checked experimentally thereafter.
The significance of the various symbols is deferred in the nomenclature to the end of this article.

2.2 Estimation of the mean fractal dimension of the flocs by laser diffractometry

Concerning methods for measuring fractal dimension, a distinction should be made between those relying on the analysis of the signal produced by an interaction between the matter and an acoustic or electromagnetic wave, and direct methods using visualisation. Among all these methods, only the light scattering technique will be presented here.

Light scattering plays an important role in the realm of textural characterization. The structural characteristics of objects, such as their size, roughness, shape and number, may be determined from diffusion curves.

The small-angle diffusion theory developed for X-rays diffractometry (DPAX) can be transposed in certain types of measurement to the scattering of neutrons or light. In all three cases, it is the contrast between the homogenous matrix and the diffusing objects that will induce an intensity diffused at small angles. This contrast will be of a diffusing nature according to the wave that is scattered. For X-rays, this contrast is caused by differences in the efficient section of the diffusion lengths; for light, it results from a variation in the refraction index. X-rays and neutrons are generally used to characterise structures smaller than one micrometer, and light, for structures on the order of one micrometer.

The intensity diffused by a group of aggregates depends on their textural variability: size and structure distributions and the nature of the objects. In the simple case corresponding to the Rayleigh-Gans-Debye (RDG) theoretical model, where the aggregate distribution in the solvent is statistically isotropic, the suspension is highly diluted so as to allow the aggregates to diffuse independently. The aggregates all have the same structure and are composed of the same basic units that verify the following optical conditions: $2\alpha|n_s - n_m| \ll 1$ and $|n_s - n_m| \ll 1$. The diffused intensity can be written

$$I(q) = K_A . C . P(q) . S(q) \qquad (23)$$

where K_A is a constant, which depends on the equipment setup and the contrast between solvent and particles. C is the particle concentration, P(q) the form factor of the particles, and S(q) the structure factor of the system. q is the amplitude of the scattering vector. It is a function of the wavelength of the incident beam, of the refractive index of dispersion medium and the scattering angle:

$$q = \frac{4.\pi.n_0}{\lambda_0} . \sin\left(\frac{\theta}{2}\right) \qquad (24)$$

For fractal aggregates, it can be shown that [16-18] the total scattered intensity will exhibit a power law dependency on q; i.e.

For $\pi/R_g \ll q \ll \pi/r_0$, $S(q) \propto q^{-D_F}$ and $I(q) \propto K_A.C.q^{-D_F}$ (25)

where R_g is the radius gyration of the aggregate, r_0 is the primary particle radius and D_F the mass fractal dimension. At length scales, approaching R_g the q^{-DF} dependence is modified by the edge of the aggregate and at small scales (approaching r_0), the non fractal nature of the constituent particles becomes apparent [10].

In principle, the relationships presented above are adequate as a description of aggregates of monosized particles only. In the more realistic case where the primary particles are polydispersed, the theory can be extended by considering the aggregates as being made of different size classes of monosized particles and accounting for each size class and its interactions with other size classes separately [19]. Dimon et al. [20] have shown that the structure factor will not be affected by polydispersity effects. The work of Tence [21], Amal and Bushell [11] shows that the fractal structure and the form of the cut-off function that describes the gross shape of the aggregates is unaffected by the details of the primary particle size distribution. It is consequently possible to determine the mean fractal dimension of the aggregates from the curve of log($I(q)$) versus log(q).
Over the interval [π/R_g , π/r_0], the curve then displays a linear segment with a slope equal to $-D_F$.

3. Material and methods

3.1 Material

The basic material used in this experiment is a commercial kaolin "Kaolin 7A", coming from the layer of Ploemeur in Morbihan in France. This material, generally employed for the coating of paper, was selected as a mineral load rather representative in term of morphogranulometry, texture and of mineralogy of the fine jets of mineral industry. From the point of view of its size distribution, this material is regarded as reference for validating the granulometric methodology of analysis of the flocs who were developed and for clearly highlighting the textural properties being able to be measured by laser diffractometry.

The preliminary characterization of this kaolin is given in Tables 1 and 2. Mineralogy was determined by X-ray diffractometry. The particle-size distribution was measured by laser diffractometry according to the optical model of Mie (MALVERN MasterSizer S) and by attenuation of X-ray (SEDIGRAPH 5100). Specific surface area of rough material and its fraction lower than 2 µm was measured by adsorption of nitrogen according to the method BET [22] by using a Micromeritics TriStar 3000 multipoint adsorptometer.

Table 1
Granulometric results of the basic material

Method	d10 (µm)	d50 (µm)	d90 (µm)	dm (µm)	DSI	% at 1 µm	% at 2 µm
PAD Laser Diff.	0.2	0.6	3.6	1.4	2.8	63.0	78.5
Sedigraph	0.1	0.7	3.2	1.2	2.2	61.2	79.7

Note. Dx, diameter corresponding to x% of cumulative undersize (x=10, 50 or 90); dm, mean diameter; dmL, mean diameter measured by laser diffractometry; DSI, distribution spreading index (an indication of the extent of size distribution, $DSI = (d_{90}-d_{10})/2 \times d_{50}$); PAD Laser Diff., projected area diameter by laser diffractometry.

Table 2
Specific surface area and mineralogical composition

Size Fraction	Wt (%)	SSA (m²/g)	Kaolinite (%)	Illite (%)	Muscovite (%)	Quartz (%)
-2 µm[a]	75	19	n.d.	n.d.	n.d.	n.d.
+2 µm[a]	25	5	n.d.	n.d.	n.d.	n.d.
Analysed head	100	15.5	91	5.3	3.4	0.6

Note. SSA, specific surface area; n.d., not determined.
[a] Size fractions separated by centrifugation

3.2 Batch flocculation reactor

A flat-bottom baffled geometry was selected as the basis laboratory experiments. The geometry is given in Fig.1a in dimensionless form. The vessel contained four regularly spaced baffles. Vessels with inner volume of 4.2 L were used during this work. The selected impeller was a two-blade radial flow turbine. Torque readouts from the mechanical stirrer were calibrated with water and a 50 wt% sucrose solution at 20°C. The resulting power curve is shown in Fig.1b. The relation between the power number and the Reynolds number is given by the empirical relationship dealt with in detail in a number of reports or publications [6-8]:

$$N_P = P1 + P2 \cdot \Re_e + P3 \cdot \sqrt{\Re_e} + \frac{P4}{\sqrt{\Re_e}} + P5 \cdot \frac{\ln(\Re_e)}{\Re_e} \qquad (26) \qquad \text{for } 500 < \Re_e < 80{,}000$$

with
$P1 = 17.22777$
$P2 = 0.00014$
$P3 = -0.06513$
$P4 = -620.10336$
$P5 = 1340.54497$

This power curve was used to determine the torque T and rotational velocity N that would dissipate a given power P_b during conditioning.
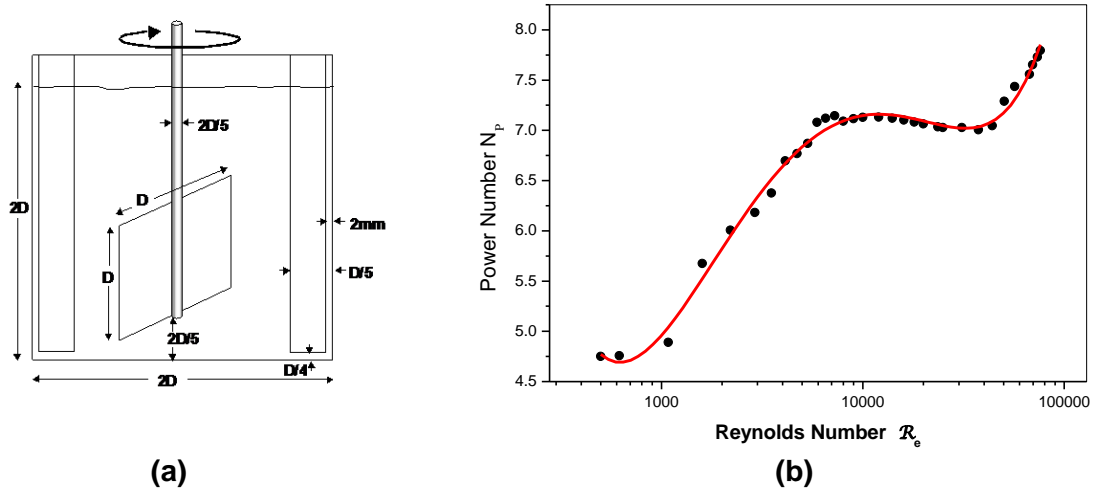

Fig.1. Laboratory conditioning system. (a) Geometrical configuration of reactor; (b) Power curve ($\mathcal{R}_e \pm 23$).

3.3 Scattering experiment set-up

The range of analysis for wet treatment provided by different particle size analysers on the market barely exceeds 900 µm. In addition to analysing finely divided materials, this range is also adapted to characterising stabilised flocs that do not exceed this limit and that can withstand the shear forces generated by the pump when the suspension is circulated in close circuit. For non-stabilized flocs, the system must run in open circuit, where the product flowing through the pump does not return to the analysis cell. Moreover, and regardless of the mode of analysis, the use of a peristaltic pump is highly inadvisable. Its pulsation propagates all the way into the cell and generates shear and a poor circulation of the pulp. In certain areas of the cell the circulation is all but stopped. This phenomenon negatively affects the reliability of the measurements. It is therefore preferable to use an open circuit driven by gravity, with a constant flow rate and, if needed, to add a centrifugal pump at the outlet. In this context, it was necessary to develop an analysis system enabling large-sized fragile flocs to be characterised – from a few micrometers to 4 mm. To do so, alterations were made to the Malvern Mastersizer-S PSA. This instrument, which lends itself well to this development, possesses a long optical bench for dry treatment analyses with a 1000 mm lens making it possible to cover a range of 4.2 to 3480 µm. To convert it for wet treatment, an analysis cell having a 10 mm optical path was built by BRGM. It was inserted in open circuit between a 4.2 litre baffled feed reactor obeying similarity for the geometric parameters indicated in the preceding paragraph (Fig. 1) and the PSA's centrifugal pump. The mixture is placed in suspension by means of the perforated impeller turning at 80 rpm ($G=20 \ s^{-1}$). The circulation takes place from bottom to top, with a flow rate of 1.8 l/min. For each analysis, the flocs retrieved in the flocculation reactor when stirring stops are placed gently in the water of the PSA reactor by means of a 'ladle' of known capacity. However, despite all the precautions taken, the structure of the macro-flocs (1 to 5mm) that formed in the flocculation reactor several moments after stirring has stopped is not preserved in the PSA reactor due to impacts between primary flocs. This methodology makes it possible to characterise in a satisfactory manner the primary flocs constituted when stirring ended, as a function of the physical and chemical and hydrodynamic conditions.

3.4 Experimental

As a preliminary to the flocculation tests, the new cell was positioned, in terms of obscuration, with respect to the classical 0.5 and 2.4 mm cells. The suspension to circulate in it must be neither too weak, in order to obtain a statistically valid representation from a large enough number of grains, nor too strong, which would induce an optical distortion and errors in the textural parameters that are measured and, in particular, in the determination of the voluminal concentration. To respect these

criteria, obscuration measurements as a function of concentration were performed for the three optical paths (0.5, 2.4 and 10 mm) on a quartz sample with a granularity range of 2 to 80 µm. The Beer-Lambert law was examined, and the critical obscurations were determined.

The flocculation of the kaolin was carried out in the reactor of flocculation indicated above. The concentration employed is 100 mg/L. The impeller velocity is fixed to 200 rpm during 15 s. The corresponding averaged velocity gradient and Reynolds number are respectively 545 s^{-1} and 24,000. Floc structure was examined in relation to the flocculant concentration (AN 934 MPM).

The values of the fractal dimensions are determined from the relationship $\log(I(q))$ versus $\log(q)$ in the range $\pi/R_z \ll q \ll \pi/r_s$ (R_z is the maximum size of aggregates and r_s is the scatterer radius), where the function is linear (Eq. (25)). Experimental observation showed that this dimension may have values ranging between 1.4 and 2.8 [23,24].

4. Results and discussions

4.1 Critical obscuration of the new cell

An examination of the volume concentration in relation to the concentration of the quartz suspension (Fig. 2) reveals the existence of a critical point corresponding to a critical obscuration above which the proportionality between C_v and C (or Ob and C) is no longer respected. Any parameter measured or determined above this point presents certainly large errors. Multiple diffusion, mask effect and optical saturation occur frequently in this zone, and evolve very significantly in relation to the actual concentration. Below this point, the size and the particle volume concentration measured by the PSA are statistically accurate. The obscuration intervals usable by the 0.5, 2.4 and 10 mm cells are respectively 3 to 18%, 3 to 20% and 3 to 28%.

4.2 Preliminary characterization

The preliminary characterization of the kaolin 7A shows that:

- This material is polydisperse. Its granulometric extent lies between 2 and 3 following the method of analysis employed.
- It contains a very large colloidal fraction in mass and a number. The estimate of this fraction is given starting from the data of the "Sedigraph" and the projected area distribution of particles obtained by laser diffractometry.
- In suspension, this material is very stable.

4.3 Flocculation of kaolin

The particle-size distributions in volume of the rough kaolin and the various tests of flocculation are given in superposition in Fig. 3. The raw kaolin curve consists of two populations centred approximately on 0.3 and 4.5 µm. The population density in volume of this latter largely exceeds that of the first population. For flocculated products and for the prevailing hydrodynamic conditions, the number of populations depends on the concentration in flocculant. For a quantification of less than 100 g/t (Fig. 3, E2 to E5), the populations are three in number. The first two, of very small amplitude, correspond to a residue of the two populations in the raw product. The third population results from the flocculation. The amplitude of the first two populations decreases, thereby contributing to increasing the third population's amplitude as the flocculant concentration increases; it tends practically towards zero from 100 g/t on. Above this dosage, the distribution consists mainly of a single population, the centre of which shifts progressively to larger sizes as the concentration in flocculant increases up to an optimum dosage of 350 g/t. Beyond this value, the centre of the population remains constant. This stabilisation is probably linked to a saturation of the sites of flocculant adsorption in the mineral. The fractal dimension, also, stabilises around 2.6, indicating a state of extreme compactness. Above 100 g/t (Fig. 3, E6 to E12), the curves can be deduced from each other by simple translation. Furthermore, the distributions become increasingly tight. These properties implicitly point to a convergence towards a monomodal population composed of compact flocs with very similar degrees of compactness. The values of average mass fractal dimension evolve in this direction as shown on Fig. 4a.

Fig. 4b, depicting the evolution of the average mass fractal dimension of mass determined by light scattering versus flocculant concentration, indicates the appearance of a floc structure that is increasingly compact. It changes from 1.2 ± 0.1, for 47 g/t of flocculant, to 2.2 ± 0.04, for 100 g/t. This range corresponds to flocs that have receptor sites still available and a structure up to 1.8 that is loose, and then increasingly compact from there on. It continues to increase up to 2.61 ± 0.03 for 340 g/t of flocculent. A further increase in quantification does not appear, at the scale of the test, to alter the internal organisation of the macro-flocs. The optimum condition in terms of concentration, determined by the intersection of two tangents, lies at 350 g/t for a D_F value of 2.61. At the scale of the test, floc architecture stabilises between 340 and 800 g/t. The behaviour of the particle size distributions is in line with these observations. In a first approximation, the relationship between D_F and DSIV (distribution spreading index in volume) is linear (Fig. 5a). Below 340 g/t, the fractal dimension increases when the spread of the DSIV distributions of the flocs decreases. Above this dosage, DSIV stabilises. This suggests the existence of an upper limit value for D_F, with the saturation of the adsorption sites and the presence of an excess of flocculant beyond the concentration corresponding to $D_{F\,MAX}$.

The analysis of the fractal behaviour in the space $\ln(\rho_F-\rho_L)$ or $\ln(1-\varepsilon_F)$ as a function of $\ln(dmL/dmL_0)$ and for concentrations of flocculant between 47 and 800 g/t indicates the existence of two families of flocs (Fig. 5b). The first family, F1, corresponds to flocs formed by the aggregation of dense micro-flocs, the structure of which becomes less and less loose as the flocculant concentration increases. The places of inking are less and less free. The fractal dimension of this family displays a linear and fairly rapid increase. The second family, F2, reflects the existence of fairly compact macro-flocs. The mean fractal dimension of the two families together is 2. The range of concentrations used does not make it possible to demonstrate the zone where micro-flocs form, situated below 47 g/t.

An investigation of Eq. (22) or (20) also enables the determination of the mean fractal dimension for all the flocculation tests, irrespective of family (Fig. 5c). The value obtained in the present case is 2. Fig. 5c also shows that floc density decreases with in creasing floc size, roughly in accordance with a power-law relationship between density and size.
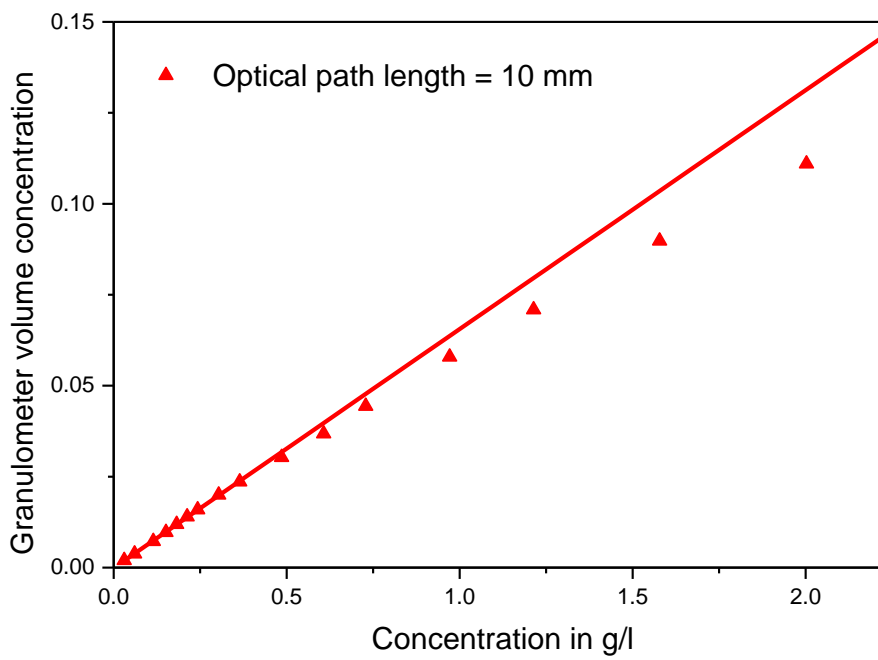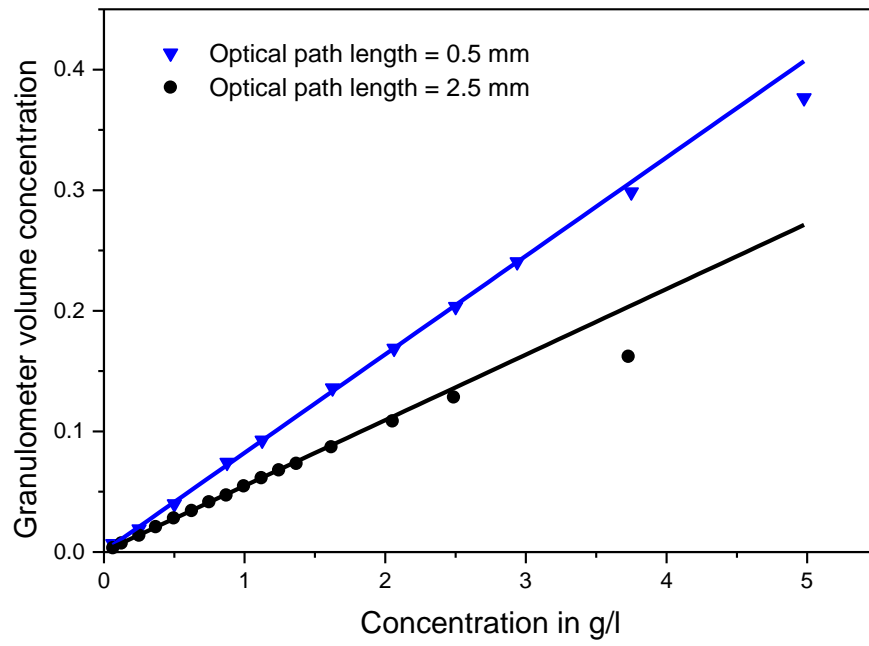
Fig. 2. Evolution of the granulometer volume concentration as a function of the concentration of solid.
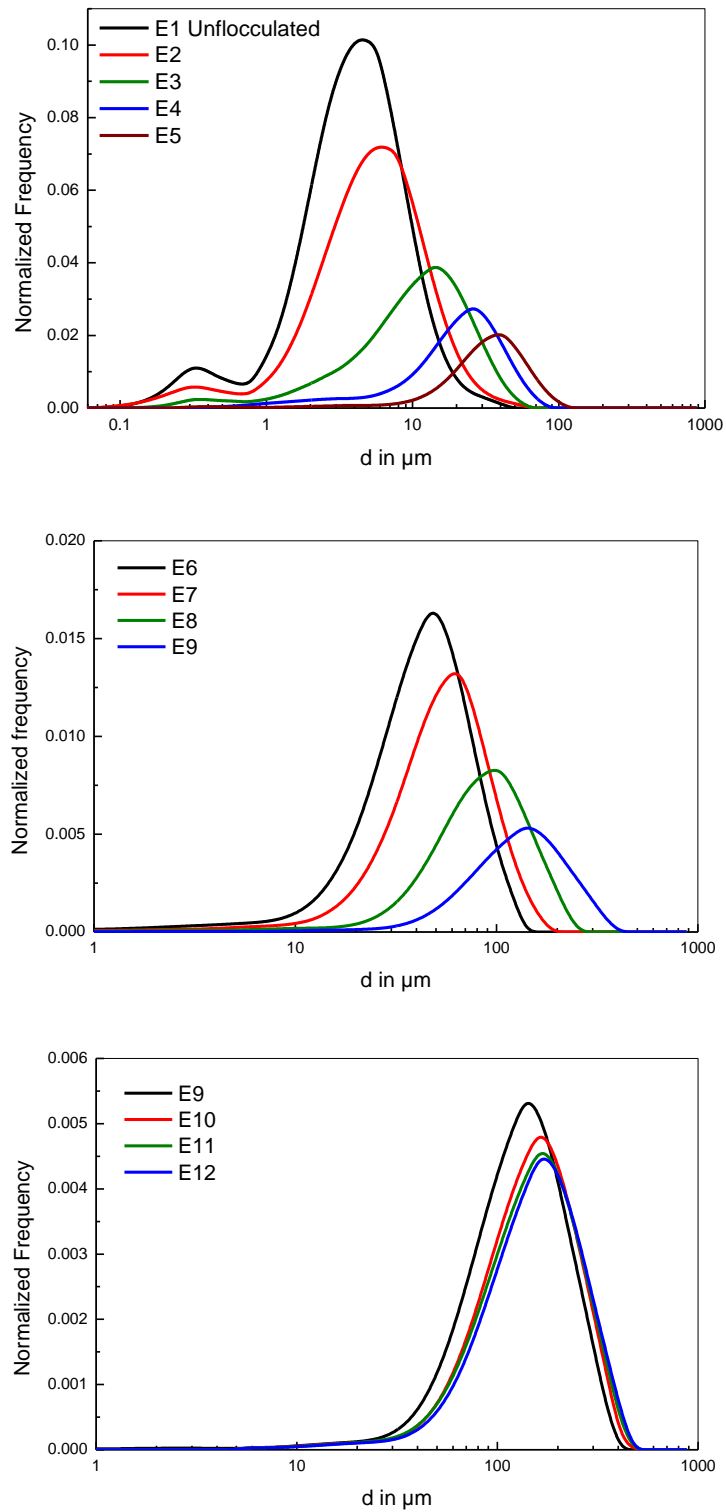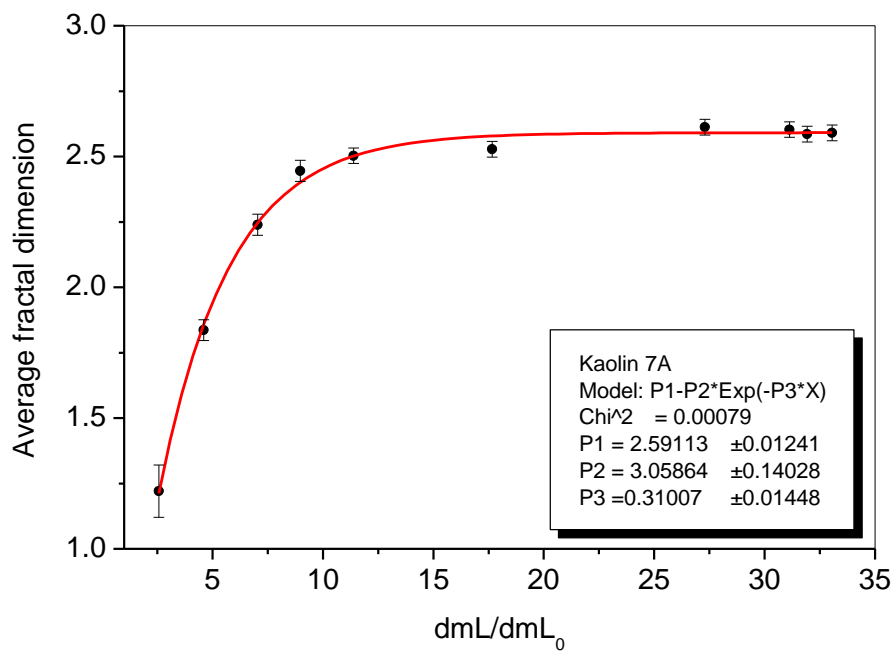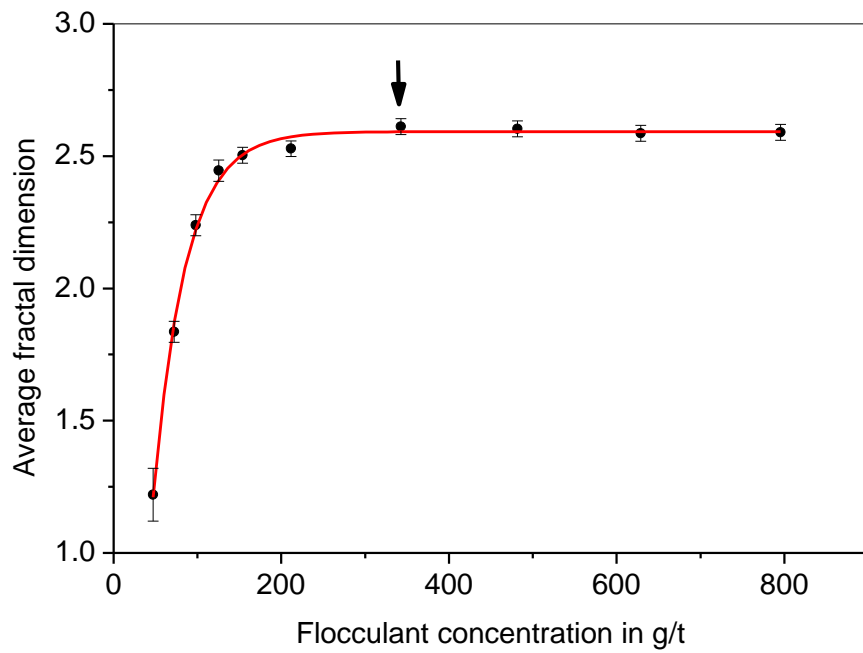
Fig. 3. Floc size distribution as a function of flocculant concentration after 15 s of stirring.

Test	E1	E2	E3	E4	E5	E6	E7	E8	E9	E10	E11	E12
CF(g/t)	0	23.2	47.2	72.2	98.2	125.4	154	211.5	343	482	629	795.4

Where CF is the concentration of flocculant in gram per ton.

Fig. 4. Evolution of the average fractal dimension as a function of the relative floc size (a), and of the flocculant concentration (b).
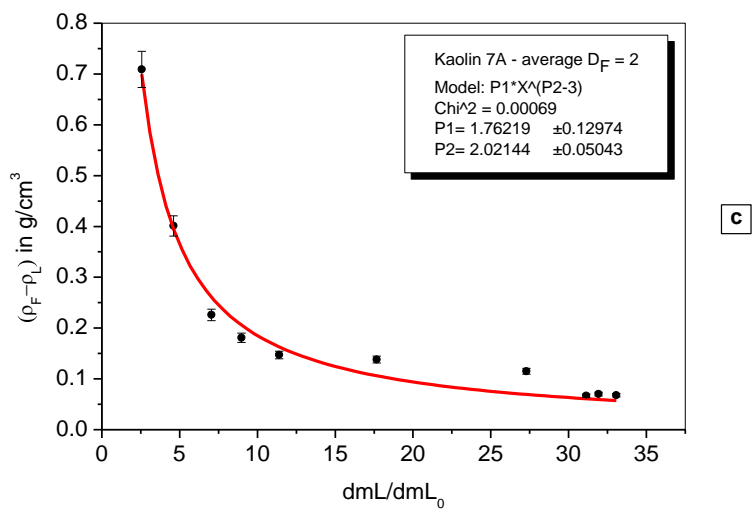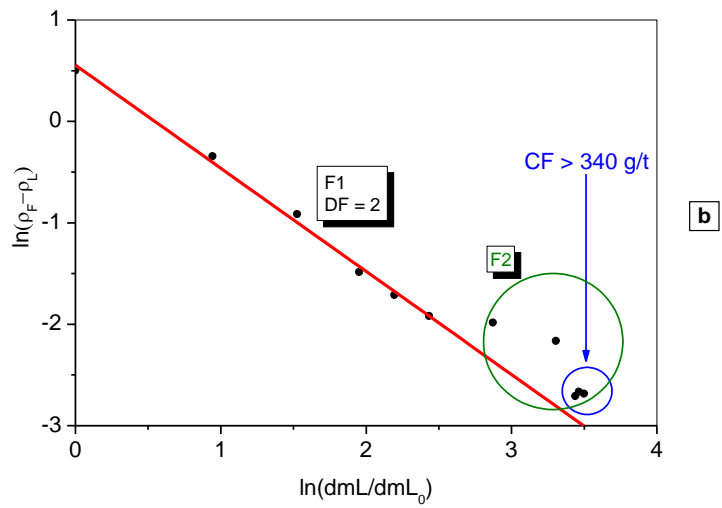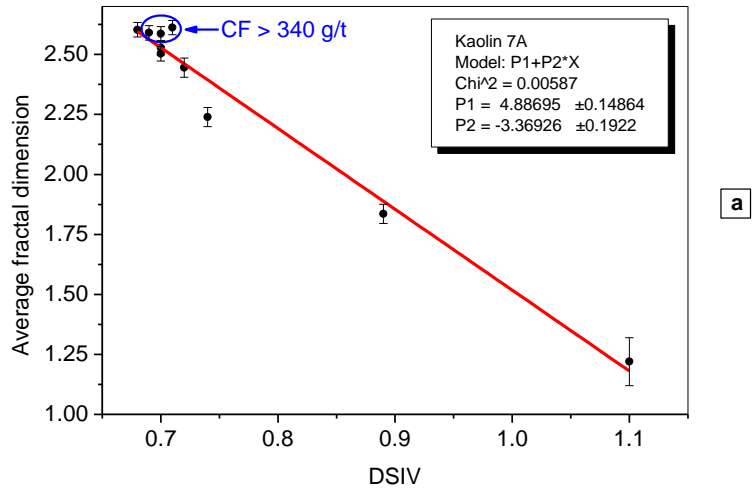
Fig. 5. Floc texture as a function of flocculant concentration

5. Conclusion

This work shows that laser diffraction particle size analysis, as a very widespread analytical tool in industrial contexts, enables certain textural characteristics to be obtained and these latter are fairly suitable to explain the macroscopic properties of a physical and chemical phenomenon.
In the realm of flocculation, as in quite a few others, the investigation of the influence of texture, determined by using this method, on the hydrodynamic behaviour of the matter makes it possible to optimise the industrial installation. To measure the thickness and the shape coefficient of lamellar particles, this technique has largely proven effective. For flocculated matter, the size, porosity and density of the flocs, as well as the volume fraction, can be obtained without restrictions due to their polydisperse nature.

For suspensions of flocs consisted of polydisperse fine particles centred on 1 µm and having a median diameter of about 0.5 µm, laser diffractometry using a wavelength of 0.632 µm is completely adapted and suitable to determine the fractal dimension of the flocs.

Aggregate density in the investigated systems decreased rapidly with increasing aggregate size. The density-size distributions can be used to obtain an accurate mass-size distribution for the flocs in an aggregated suspension.

Appendix A. Nomenclature

A_i	projected area of the size band i;
C	concentration expressed as grams per millilitre;
C_V	particle volume concentration measured by the granulometer (volume of all particles per volume of suspension containing these particles);
d_0	particle diameter;
d_i	diameter of the size band i;
$d_{3.2}$	Sauter mean diameter;
D_F	average fractal dimension;
d_m	mean diameter;
d_{mL}	floc mean diameter measured by laser diffractometry;
d_{mL0}	mean diameter of the elementary particles measured by laser diffractometry;
DSI	Distribution spreading index;
I	total scattered intensity;
I_c	intensity received on central detecror;
I_0	intensity emitted by the laser (received in absence of particles);
k	wave number ($k=2\pi/\lambda_0$);
k_0	fractal prefactor, which is a function of the average size of primary particle ;
K_A	constant depending on the apparatus and on the optical contrast between scatteres and their environment;
ℓ	optical path length;
n	number of primary particles in an aggregate;
n_s	refractive index of the scatterers;
n_m	refractive index of the propagating medium;
N	impeller rotational speed;
N_i	number of particles of size band "I" per unit volume;
N_P	dimensionless power number;
Ob	obscuration of the light;
P(q)	function of the form factor;
q	modulus of the scattering wave-vector;
$Q_{ext,i}$	extinction efficiency (for Fraunhofer diffraction, it is equal to 2);
$\overline{Q_{ext}}$	average extinction efficiency;
r_0	radius of the primary particle (monodisperse);
R	radius of the aggregate;
R_g	radius of gyration of the aggregate;
S(q)	structure factor;

SSA   specific surface area BET;

TEM$_{00}$ transversal electric and magnetic wave, where the subscripts "00" refer to a cylindrical Gaussian irradiance;

V$_B$ beam volume which is the cross-sectional area times the path length;

V$_i$ volume of particles in size band i per unit volume;

V$_0$ volume of an elementary particle;

V$_P$ volume of the suspension;

V$_{ri}$ relative volume of particles in size band i per unit volume;

V$_{SB}$ total volume of all solid scattering particles in the beam;

V$_{SR}$ real volume of the solid.

Greek symbols

α size parameter;

ε_F average floc porosity;

θ scattering angle;

λ_0 light wavelength in vacuum;

ρ_S density of particulate matter expressed as grams per cm^3;

ρ_F average floc density (g/cm^3);

ρ_L fluid density (g/cm^3);

ρ_S density of particulate matter (g/cm^3);

τ particle field turbidity;

Φ_F solid volume fraction.

References

[1] S. Veerapaneni, et al., J. Colloid Interface Sci., 177 (1996) 45.

[2] G.W. Chen, et al., Water Research, 30(8) (1996) 1844.

[3] K. Grijspeerdt et al., Water Research, 31(5) (1997) 1126.

[4] M.R. Wiesner, Water Research, 26 (1992) 379.

[5] B.W. Brandt et al., *Biotech. & Bioeng* 70 (2000) 677.

[6] T. Allen, Powder Technology series Chapman and Hall. (1974).

[7] G. Baudet et al., Spectra 2000, 132, 16 (1998) 37.

[8] G. Baudet et al., Particulate Science and Technologie 11 (1993) 73.

[9] M. BIZI et al., European Journal of Pharmaceutical Sciences 19 (2003) 373.

[10] J. Guan, R. Amal, T.D. Waite, Proceedings of the 26th Australasian Chemical Engineering Conference (Chemeca 98), Port Douglas, Australia 1998.

[11] R. Amal, G. Bushell, J. Colloid and Interface Sci. 205 (1998) 459.

[12] M. Lattuada et al., Physical Review E, 64 (2001) 061404.

[13] J. Swithenbank et al., AIAA 14th Aerospace science meeting, Washington D.C. 1976.

[14] H.C. Van de Hulst, Dover Publications, Inc., New York. Systems Yearbook, 6 (1981) 131.

[15] R.B. Penndorf, J. Opt. Soc. Amer., 52 (1968) 896.

[16] M. Kerker, Academic Press, New York, 1969.

[17] A. Guinier, et al., Wiley: New York, 1955.

[18] C.F. Bohren et al., Wiley: New York, 1983.

[19] P. Salgi et al.,Adv. Colloid Interface Sci.43 (1993) 169.

[20] P. Dimon, Phys. Rev. Lett.57 (1986) 595.

[21] M. Tence et al., J. Phys. 47 (1986) 1989.

[22] F. Rouquerol et al., Academic Press, 1999, p. 165.

[23] M.A.V. Axelos et al., J. Physique, 47 (1986) 1843.

[24] Ganczarczyk, Water Science and Technology, 30(8) (1994) 87.